Journal of Nuclear Materials 377 (2008) 182–188

Contents lists available at ScienceDirect

Journal of Nuclear Materials

journal homepage: www.elsevier.com/locate/jnucmat

Cavitation damage prediction for spallation target vessels by assessment of acoustic vibration

Masatoshi Futakawa [a,*], Hiroyuki Kogawa [a], Shoichi Hasegawa [a], Yujiro Ikeda [a], Bernie Riemer [b], Mark Wendel [b], John Haines [b], Günter Bauer [c], Takashi Naoe [a], Kohei Okita [d], Akiko Fujiwara [e], Yoichiro Matsumoto [e], Nobuatsu Tanaka [f]

[a] J-PARC Center/JAEA, Tokai-mura, Ibaraki-ken 319-1195, Japan
[b] Spallation Neutron Source/ORNL, P.O. Box 2008, Bldg. 8600, MS 6473, Oak Ridge, TN 37831, USA
[c] Forschungszentrum Jülich, Leo-Brandt-Str., 52425 Jülich, North Rhine-Westphalia, Germany
[d] RIKEN, Wako-shi, Saitama-ken 351-0198, Japan
[e] The University of Tokyo, Hongou, Bunkyou-ku, Tokyo 113-8656, Japan
[f] Ibaraki University, Hitachi-shi, Ibaraki-ken 316-8511, Japan

ABSTRACT

Liquid-mercury target systems for MW-class spallation neutron sources are being developed around the world. Proton beams are used to induce the spallation reaction. At the moment the proton beam hits the target, pressure waves are generated in the mercury because of the abrupt heat deposition. The pressure waves interact with the target vessel leading to negative pressure that may cause cavitation along the vessel wall. In order to estimate the cavitation erosion, i.e. the pitting damage formed by the collapse of cavitation bubbles, off-beam tests were performed by using an electric magnetic impact testing machine (MIMTM), which can impose equivalent pressure pulses in mercury. The damage potential was defined based on the relationship between the pitting damage and the time-integrated acoustic vibration induced by impact due to the bubble collapses. Additionally, the damage potential was measured in on-beam tests carried out by using the proton beam at WNR (Weapons Neutron Research) facility in Los Alamos Neutron Science Center (LANSCE). In this paper, the concept of the damage potential, the relationship between the pitting damage formation and the damage potential both in off-beam and on-beam tests is shown.

1. Introduction

High-power liquid-mercury target systems for high-intensity pulsed spallation neutron sources are being developed as taking advantage of a forced flow for better heat removal and increased neutron yield. The Japan Atomic Energy Agency (JAEA) and High-Energy Accelerator Research Organization (KEK) are carrying out research and development for the JSNS (Japanese Spallation Neutron Source) aiming at basic research in materials and life sciences in J-PARC (Japan Proton Accelerator Research Complex) project [1,2]. The twin project SNS (Spallation Neutron Source) has recently been commissioned at ORNL (Oak Ridge National Laboratory). JSNS and SNS collaborate on issues of joint interest. Through our R&D collaboration on high-power mercury targets, cavitation erosion damage, the so-called pitting damage, was confirmed in mercury target vessels [3,4]. That is, the moment the proton beam hits the target vessel, stress waves will be imposed on the beam window and pressure waves will be generated in the mercury by the abrupt heat deposition [5,6]. Provided that the negative pressure causes cavitation in the mercury, the following collapses of the cavitation bubbles generate microjets and/or shock waves [7] forming micro-pits on the surface of the vessel wall [3,8]. This cavitation erosion damage accumulates on the surface of the vessel wall, compromising the structural integrity and reducing the life of the target vessel [9–11].

An electric magnetic impact testing machine, MIMTM was developed to examine the pitting damage, caused by the impulsive pressure exerted on mercury [10]. The relationships between the number of imposed pressure cycles, the deposited power and pitting damage, etc. have been investigated systematically using the MIMTM. An in situ monitoring system is being developed as a diagnostic system for the detection of abnormal events during operation of the high-power mercury targets and to accumulate data associated with the damage of the target structure. Several indirect methods to evaluate cavitation erosion and surface vibration in structures have been proposed using accelerometers, hydrophones, acoustic emission sensors, [12,13] and laser Doppler vibrometers [14]. Acoustic vibration measurement using a laser Doppler system is available and further attractive technology in neutron radiation

---

[*] Corresponding author.
E-mail address: futakawa.masatoshi@jaea.go.jp (M. Futakawa).

0022-3115/$ - see front matter © 2008 Elsevier B.V. All rights reserved.
doi:10.1016/j.jnucmat.2008.02.058

environments to evaluate dynamic phenomena [6,15]. Acoustic vibration measurements were carried out in the MIMTM tests under various conditions: the number of impact cycles, repetition rate and deposited power. This type of measurement was also carried out in the on-beam test using the proton beam at the WNR (Weapons Neutron Research) facility at the Los Alamos Neutron Science Center (LANSCE). In this paper, the damage potential evaluated by the acoustic vibration will be presented and compared with the optically observed pitting damage to examine the possibility of an in situ monitoring system as a diagnostic system for the detection of abnormal events and for the assessment of the structural integrity of the target.

2. Experimental

2.1. Off-beam test

The MIMTM (Max. acc.: ca. 300 g) was developed to examine the pitting damage formation for more than 10 million cycles. As shown in Fig. 1, a short cylinder is filled with ca. 120 cc of mercury. The impulsive pressure is repeatedly imposed at 25 Hz through a disk specimen driven by the striker. The pitting damage was formed on the contacting surface with mercury of the disk specimen of type 316 stainless steel, 316ss. The imposed pressure was precisely and quantitatively controlled by changing supplied electric power for the magnet coils. The pressure was measured by a pressure gage (Entran EPXH) fixed on the lid of the mercury chamber. The more detailed description was reported elsewhere [10].

The acceleration induced by acoustic emissions of collapsing micro-bubbles was measured by using a piezo-type accelerometer (RION PV-90B) that was fixed on the striker. The signals of acceleration were digitally recoded at a sampling rate of 1 μs and filtered within different frequency ranges to estimate the damage potential related to the pitting damage. The effects of deposited power on the damage formation were investigated in the ranges from 150 W to 560 W. The morphology of the pits observed at 560 W in MIMTM was determined to be similar to that observed from the WNR mercury target experiments using a proton beam with intensity equivalent to the 1 MW beam in the SNS [10].

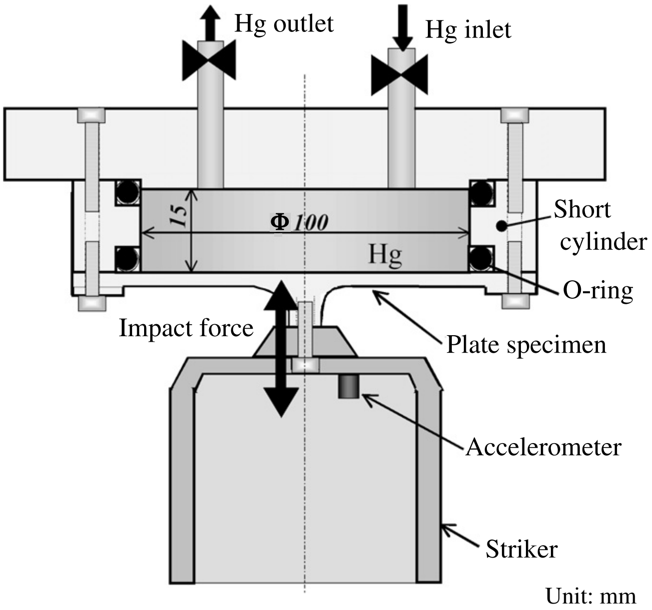

Fig. 1. MIMTM chamber for mercury. The impact pressure is imposed on the mercury in the chamber through the plate specimen.

The morphology of the pits on the disk specimen surfaces was examined using a confocus laser microscope (Laser tech. LHD-15 H). The analyzed images were digitized to quantitatively evaluate the area damaged by pits. The pits with depth of more than 0.5 μm were defined to be the damage. Damage was evaluated as a ratio of damaged area to observed area [10].

2.2. On-beam test

The on-beam tests using a small mercury test loop that applied 100 proton beam pulses with ca. 2.6×10^{13} protons per pulse for each test condition were performed. The cross-section of the test loop was 50×25 mm^2 and the flange-type damage test specimens fabricated from annealed type 316L stainless steel were installed as beam windows, as seen in Fig. 2. The detection of the displacement velocity of the pipe wall of the tests loop was carried out using a laser Doppler system (Onosokki LV1720). The measuring points are at 3 mm (position A) and 15 mm (position B) from the center of the proton bombarded area in the down-stream direction of mercury flow. The measurements were carried out for various flow conditions: no flow, flow at 0.4 m/s and flow at 0.4 m/s combined with helium gas bubbling. Unfortunately, the bubble size and void fraction could not be measured. More detailed information regarding the test loop is reported elsewhere [16]. The damage observation of the flange type specimens was carried out at ORNL using a SEM (scanning electron microscopy).

2.3. Damage potential

Internal microjets which may impinge on the walls of the vessel are generated by cavitation bubble collapse. The impact responses exhibit various frequency components. Fig. 3 shows the acceleration response measured for a deposited power of 560 W in the MIMTM. The corresponding velocities and displacements were obtained by integration of the acceleration data. Assuming that the pressure generated in the mercury around the surface of the disk specimen is associated with the displacement, the negative pressure appears just after the impact of the striker and reaches its minimum value at about 2 ms. High-frequency components are superimposed on the acceleration response just after the minimum pressure appearance. Fig. 4 shows the frequency spectrum of the acceleration response shown in Fig. 3. The high-frequency components above

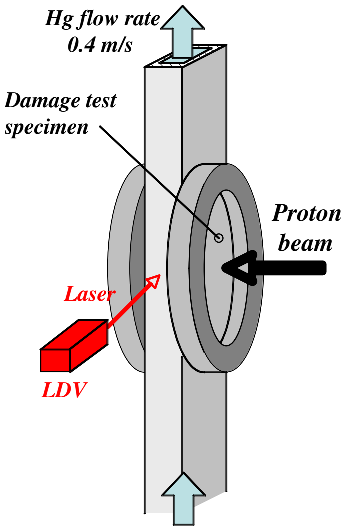

Fig. 2. Schematic drawing of test section of mercury loop used at WNR test. Mercury flows in the rectangular pipe, cross-section 50 mm × 25 mm, under various conditions: no flow, flow, flow with bubbles.

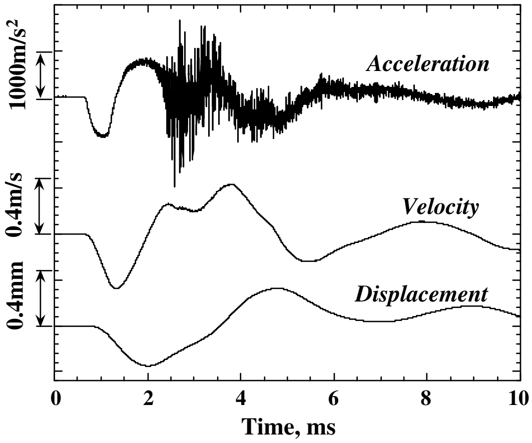

Fig. 3. Time-responses of acceleration, velocity and displacement of the striker. Velocity and displacement were obtained by integration of the acceleration response.

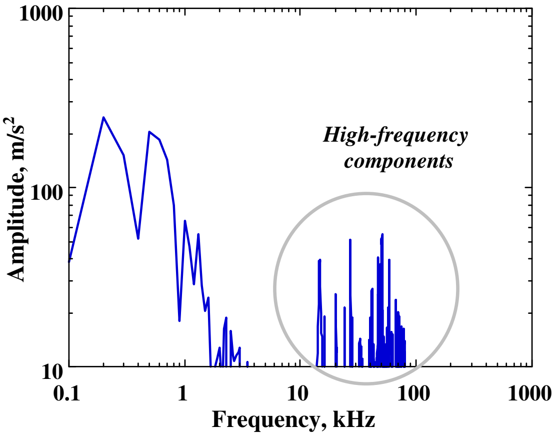

Fig. 4. Frequency spectrum of acceleration response in Fig. 3.

15 kHz are recognized at 560 W, but are not observed in the acceleration response measured for powers lower than 185 W corresponding to the fact that no pits were observed afterwards on the plate specimen. The high-frequency components were extracted by using the high-pass filter above 15 kHz, as illustrated in Fig. 5. These components are due to the localized impacts caused by collapsing micro-bubbles, which result in the pit formation. In order to quantitatively evaluate the correlation between the acceleration $a_i(t)$ with high-frequency components and the pitting damage, the E value associated with the impact energy by micro-bubble collapsing during an pressure impulse is defined by the following equation:

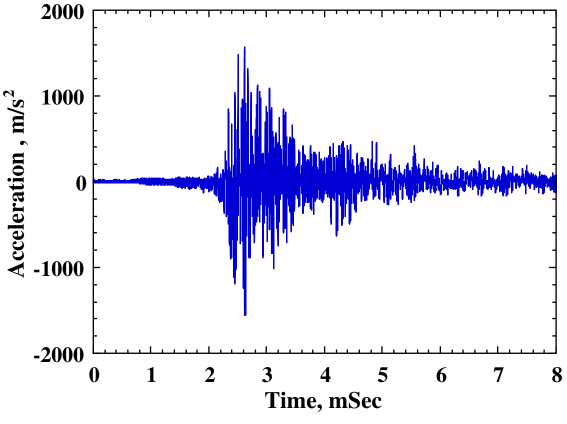

Fig. 5. High-frequency components extracted by high-pass-filtering.

$$E = \sum_{i}^{n} \left(\int_{0}^{\Delta t} |a_i| \mathrm{d}t \right)^2, \tag{1}$$

where n is the number of localized impacts during one pulse and Δt is the impact period. The damage potential φ is therefore defined by

$$\phi = (E - E_{\mathrm{th}}), \tag{2}$$

where E_{th} is a threshold value for damage.

In the on-beam tests, however, we used the laser Doppler vibrometer (LVD) to estimate the damage potential because the electric signal obtained from the accelerometer would be affected by the proton beam injection [6]. Then, Eq. (1) is given by

$$E = \sum_{i}^{n} |V_i|^2, \tag{3}$$

where V_i is the velocity of displacement measured by using the LDV.

On the other hand, the low-frequency components below 15 kHz, correspond to the dynamic responses describing the macroscopic vibrational behavior.

3. Results

3.1. Off-beam tests by MIMTM

The number of pulses and the imposed power were systematically changed to investigate the dependence of the pitting damage on the number of impulsive impacts. The damage potential was evaluated under various conditions. We define the accumulative damage potential φ_{a} by

$$\phi_{\mathrm{a}} = \sum_{j}^{N} \phi_j^{\mathrm{p}}, \tag{4}$$

where ϕ_j^{p} is the damage potential at the jth pulse with the imposed power p, N the number of pulses.

The relationship between the fraction of eroded area A_{e}/A_0 in the damaged specimens and the normalized accumulative damage potential $\varphi_{\mathrm{a}}/\varphi_{\mathrm{a0}}$ is plotted logarithmically in Fig. 6. Here, φ_{a0} is φ_{a}

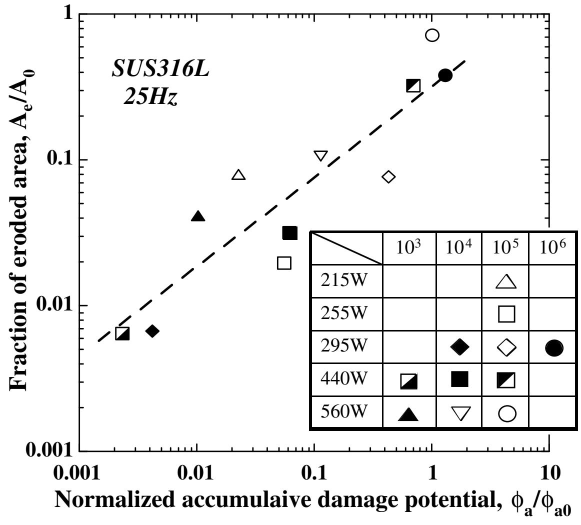

Fig. 6. Relationship between A_{e}/A_0 and $\varphi_{\mathrm{a}}/\varphi_{\mathrm{a0}}$. The slope of the best fit line is $m = 0.6$ in Eq. (5).

after 10^5 cycles at 560 W. It is confirmed from Fig. 6 that the damage potential can be calculated to estimate the fraction of the eroded area independently from the deposited power and the number of pulses, and the relationship between A_e/A_0 and φ_a/φ_{a0} is approximately given by

$$\frac{A_e}{A_0} = C_1\left(\frac{\phi_a}{\phi_{a_0}}\right)^m = C_1\phi_n^m, \tag{5}$$

where C_1 and m are constants; for these test conditions, $C_1 = 0.3$ and $m = 0.6$ for 316ss. The damage formation in the incubation period may be predicted by using Eq. (5) if the damage potential is known.

3.2. On-beam test at WNR

Fig. 7 shows typical results of the velocities of the pipe wall at position A and B under each condition: i.e. no flow, flow, and flow with bubbles, which were measured at positions A and B. The high-frequency components are more pronounced in the velocity signal with no flow compared to the other two cases. The velocity with the bubbly flow is almost damped to zero around 1 ms, while those without bubbles continue vibrating even after 2 ms.

Fig. 8 shows the frequency spectrum of the displacement velocity obtained by averaging all measured waves for each condition. In the frequency range below 15 kHz the amplitude for the bubbly flow is lower than for the other cases without bubbles and the difference between flow and no flow conditions is hardly recognized, in particular, for frequencies lower than 5 kHz.

Fig. 9 shows the dynamic responses under each condition, which were extracted by low-pass-filtering with lower than 15 kHz. The first peaks with a cut-off frequency of 15 kHz appear at around 0.05 ms after the beam injection and then the minimum peaks around 0.18 ms. The minimum peak for bubbly flow is reduced by almost a factor of 2 compared to the other cases. Also, the first appearing peak is delayed for the bubbly flow. It is confirmed from Figs. 8 and 9 that the presence of the bubbles reduces the amplitude at the frequency range lower than 15 kHz, so-called dynamic responses of the pipe wall, and that the flow hardly affects the dynamic response.

Fig. 10 shows the high-frequency components of the displacement velocity shown in Fig. 7, which were obtained by using high-pass-filtering with higher than 15 kHz. The amplitude of the high-frequency components for the stagnant mercury is higher than in the other cases. As a result, it can be said that the injected

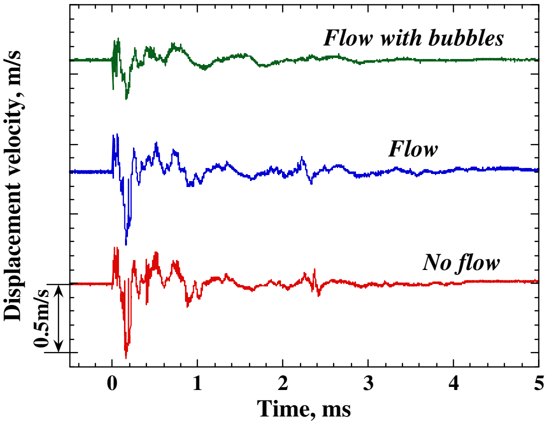

Fig. 7. Velocities of displacement measured at the pipe wall at point B under each condition: no flow, flow, flow with bubbles. The minimum peak at about 0.2 ms is smaller for the flow with bubbles than for the other conditions. The vibrations for the flow with bubbles are almost damped to zero after 1 ms, while the vibrations for the other cases persist even after 2 ms.

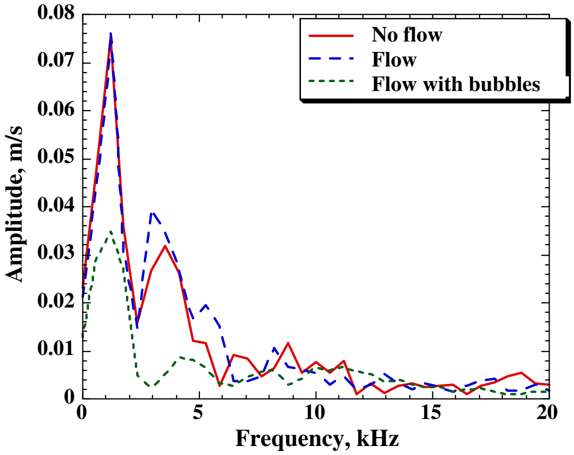

Fig. 8. Frequency spectrums of velocity of displacement. In the frequency range below 15 KHz, the amplitude for the flow with bubble is lower than in the other two cases, which can hardly be distinguished, in particular for frequencies lower that 5 KHz.

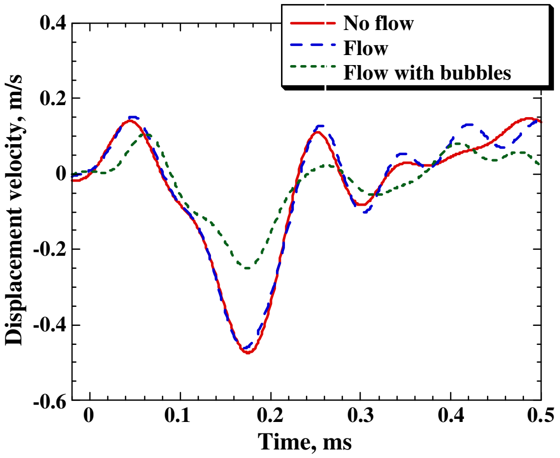

Fig. 9. Dynamic response of the pipe wall for three different conditions. The first peaks appear around 0.05 ms after the beam injection and then the minimum peaks around 0.18 ms. The minimum peak for the flow with bubbles is reduced by a factor of about 2 compared to the other cases.

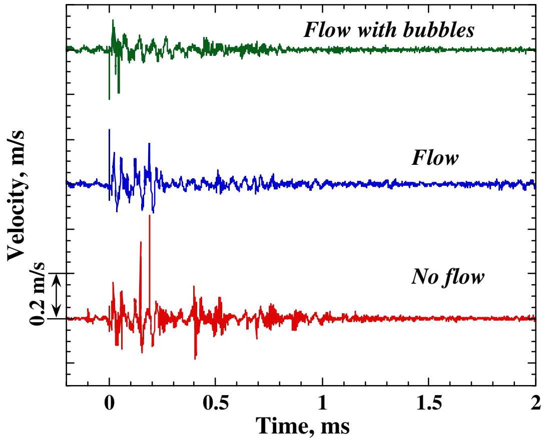

Fig. 10. High-pass-filtered velocity. The amplitude of high-frequency components without mercury flow is highest.

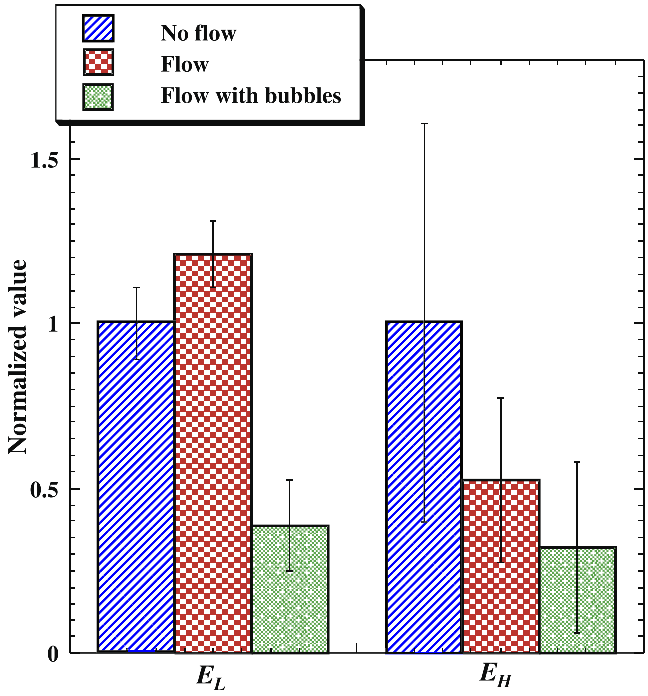

Fig. 11. E value distributions calculated from the high-frequency components. E_L is clearly reduced by bubbles, while E_H is reduced by flow regardless of whether it contains bubbles or not.

Table 1
Results on damaged specimen observation at WNR test

Test condition	Fraction of eroded area, A_e/A_0	E_H value
Stagnant	0.10	1.535
Flowing	0.065	0.769
Flowing with bubbles	0.051	0.533

bubbles reduce the magnitude of pressure wave and the dynamic response of the pipe wall in our experiment.

The E_L and E_H values correspond to the low-pass and high-pass filtered velocity according to Eq. (3). We measured ca. 100 waves at position A for each condition, which were used for statistical results. The mean values of E_L and E_H with standard deviation were plotted in Fig. 11. Each value was normalized by those obtained at no flow condition. E_L is clearly reduced by bubbling. While, E_H calculated from the high-frequency component, which is related to the micro-impact energy to form pitting damage, is reduced by the flow with bubbles or without bubbles.

Table 1 shows the fraction of the eroded area, which was evaluated by observation of the damaged specimens [16] and E_H value. The same trend to test condition was recognized between them. In the next section, we will discuss the trend in detail.

4. Discussion

Let us consider how we can predict the pitting damage in the on-beam condition from the acoustic vibration obtained by using the LDV. In the off-beam condition, the MIMTM test, the damage was estimated adequately by using Eq. (2) and $m = 0.6$ in Eq. (5) to relate the damage potential to the observed damage. Unfortunately, in the on-beam tests it is very difficult to precisely estimate the threshold value E_{th} in Eq. (2), so that the damage potential given by Eq. (2) cannot be derived directly. Nevertheless, if E_{th} is assumed to be small enough, the damage potential might be given by

$$\phi = E. \tag{6}$$

Then, Eq. (5) is rewritten as following,

$$A_e/A_0 = C/E^m. \tag{7}$$

In the case of MIMTM, E_{th} is <1% of E_H for an input power of 560 W in MIMTM, which yields a very similar morphology of the pits to that observed in the MW-class on-beam tests. The data given in Table 1 are logarithmically plotted in Fig. 12. The trend between A_e/A_0 and E_H is quite similar to that shown in Fig. 6, and $m = 0.6$, which is coincident between the off-beam and the on-beam tests. As a result, it can be said that the acoustic vibration measurement is quite useful as an in situ diagnostic system to predict the pitting damage induced by the pressure waves due to the proton beam bombardment.

In the on-beam tests, the effect of gas bubble injection was recognized from the viewpoints of the acoustic vibration and the observed damage. But, unfortunately the bubble population characteristics were unknown. The mitigation of beam induced pressure waves will be strongly effected by the bubble size distribution and void fraction [17]. In order to understand the pressure mitigation by bubbles and to predict what condition is most effective to reduce the amplitude of the pressure waves, three kinds of numerical simulations are carried out as illustrated in Fig. 13; i.e. macro, meso and micro-scales. In the macro scale, the interaction between the target structure and the mercury including pressure wave propagation is evaluated by using a conventional FEM code e.g. ABAQUS or DYNA. From these simulations we understand the period of negative pressure imposing on the target vessel wall, which is one of the important parameters for cavitation bubble formation [18].

For the meso-scale, we developed a code, PAC-MT [17] to simulate the mitigation effect of pressure waves by the bubbles injected into mercury. A typical result is shown in Fig. 14. The peak pressure at the center of the bombarded area is reduced by the bubbles, and the mitigation effect is distinguished by relatively small bubbles with less than 100 μm in diameter and void fraction of more than 0.3%. In the on-beam tests, assuming that the peak pressure is proportional to the amplitude of the dynamic response related to E_L, the peak pressure was reduced by about a factor of 2 by the presence of injected gas bubbles, as shown in Fig. 11.

Cavitation bubbles grow under negative pressure which is generated near the target vessel wall by the interaction between the

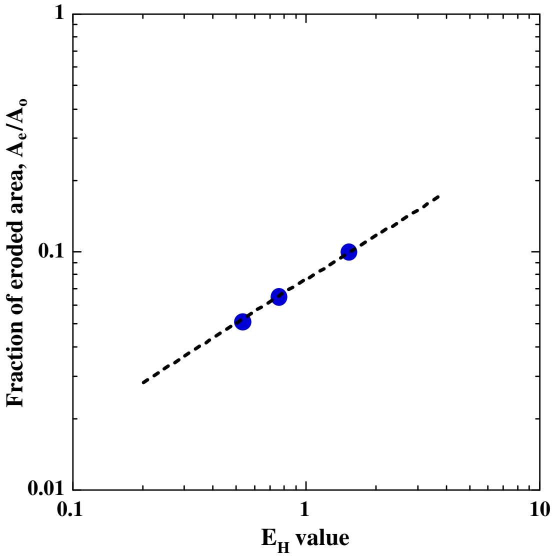

Fig. 12. A_e/A_0 and E_H at WNR tests. The slope of the fitting line is $m = 0.6$ in Eq. (7), which is coincident with the value in Eq. (5) obtained in the off-beam tests.

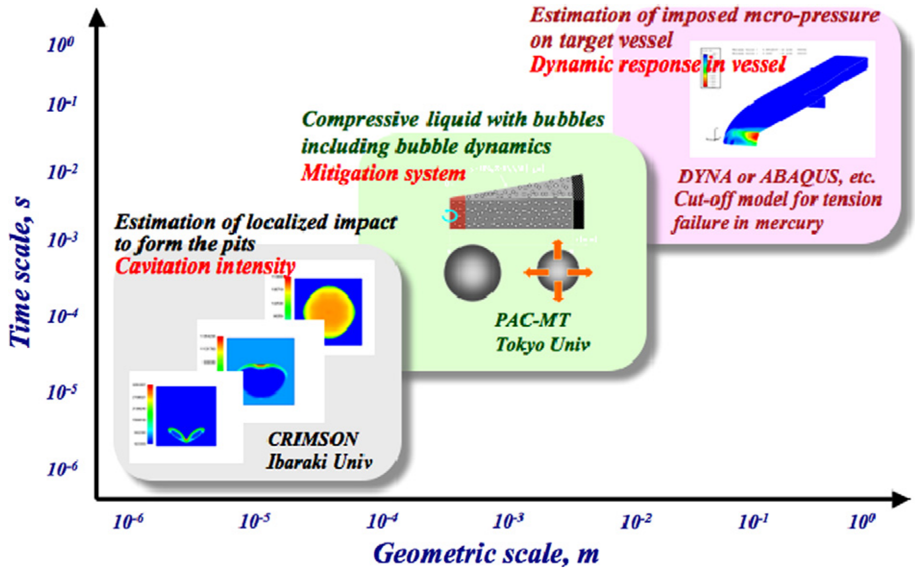

Fig. 13. Approach to the numerical simulation to understand the cavitation behavior in the mercury target. Three kinds of numerical simulations spanning three length scales (macro-, meso-, micro-scale) to understand the bubbling mitigation mechanism and predict what condition is most effective to reduce the amplitude of pressure waves.

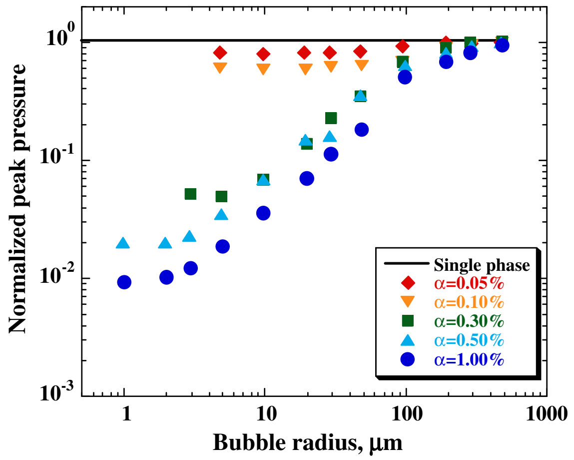

Fig. 14. Effect of bubbles on peak pressure. The peak pressure at the center of the bombarded area is reduced by the bubbles, and the mitigation effect is induced by relatively small bubbles with less than 100 m in diameter and a void fraction of more than 0.3%.

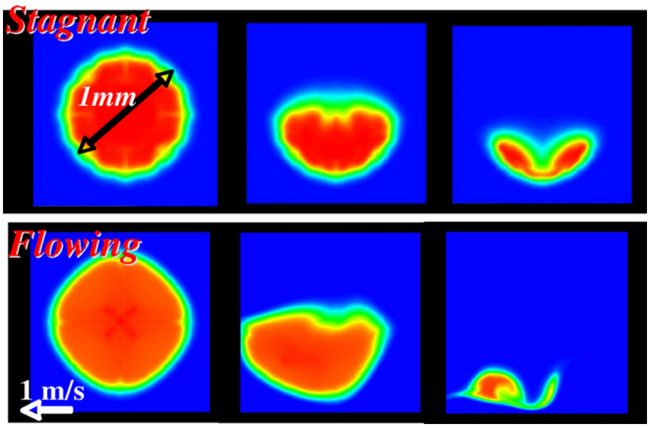

Fig. 15. Simulated bubble collapse in stagnant and flowing condition. Preliminary simulations were carried out taking into account the vapor pressure, viscosity, surface tension of mercury, etc. The collapse behavior is affected by the mercury flow.

target vessel and pressure waves. Cavitation bubble growth is very dependent on the negative pressure behavior, that is, the period and amplitude of the pressure. The aggressiveness of cavitation bubble is affected by the negative pressure. The bubble injection should influence not only the beam-induced compressive pressure but also the negative pressure. We are investigating the dynamic response of the negative pressure induced by the interaction between the solid and liquid metal taking into account the effect of injected gas-bubbles using the meso-scale model.

In the micro-scale, a novel code based on a finite-volume method combined with the high-order interpolation scheme, CRIMSON [19], was developed to understand the effects of the mercury flow and the duration of the pressure waves on the cavitation-bubble collapse behavior. Preliminary simulations were carried out taking into account the mercury properties such as vapor pressure, viscosity, surface tension, etc. as shown in Fig. 15. The collapse behavior is affected by flowing mercury. At present, the simulation does not provide sufficient quantitative information on micro-impact due to the cavitation bubble collapse. We will improve the code to quantitatively estimate the velocity of microjets and their force onto the wall [20]. The reduction of $E_{\rm H}$ observed in the on-beam test may be due to the change in cavitation bubble collapse behavior by mercury flow characteristics, as suggested in Fig. 15.

5. Conclusion

MW-class spallation mercury-target systems for next generation neutron sources will suffer from cavitation damage. Such damage is a crucial issue which will adversely effect the lifetime and structural integrity of the targets. So far, the off-beam tests have been systematically carried out to understand the damage formation and the degradation of target wall materials due to cavitation damage. Additionally, the on-beam tests were carried out at the WNR facility in LANSCE. In both the off-beam and on-beam tests it was found that the cavitation damage is predicted by the damage potential calculated from acoustic vibration which due to the impact from cavitation bubble collapse. The acoustic vibration measuring technique using a laser Doppler vibrometer will be useful as an in situ diagnostic system for mercury targets in high-radiation environments. The presence of bubbles may be effective for mitigating the pressure waves in mercury targets and for reducing the pitting damage. The effect and condition of injected gas-bubbles into mercury on the mitigation were evaluated through numerical simulations performed in three size scale models; macro, meso and micro-scales. The aggressiveness of cavitation bubbles depends on the negative pressure behavior. From this viewpoint, we will carry out the simulations to understand the effect of injected gas-bubbles on the negative pressure induced by the interaction between solid and liquid metals.

Acknowledgements

The authors would like to thank Emeritus Professor N. Watanabe of JAEA for his fruitful advice and encouragement to this research work. This work was partly supported by Japan Society for the Promotion of Science under Grant-in-Aid for Scientific Research 17360085 and 17560740.

References

[1] S. Nagamiya, Neutron News 16 (1) (2005) 16.
[2] Y. Ikeda, Neutron News 16 (1) (2005) 20.
[3] M. Futakawa, H. Kogawa, R. Hino, J. Phys. IV France 10 (Pt 9) (2000) 237.
[4] J.R. Haines, K. Farrell, J.D. Hunn, D.C. Lousteau, L.K. Mansur, T.J. McManamy, S.J. Pawel, B.W. Riemer, SNS-101060100-TR0004, 2002.
[5] K. Skala, G.S. Bauer, in: ICANS XIII, 1995, p. 559.
[6] M. Futakawa, K. Kikuchi, H. Conrad, H. Stechemesser, Nucl. Instrum. and Meth. A 439 (2000) 1.
[7] For example: D. Lohse, Phys. Today (2003) 36.
[8] J.M. Carpenter, IWTTHHLM, Schruns, Austria, 1996.
[9] M. Futakawa, H. Kogawa, R. Hino, H. Date, H. Takeishi, Int J. Imp. Eng. 28 (2003) 123.
[10] M. Futakawa, T. Naoe, H. Kogawa, C. Tsai, Y. Ikeda, J. Nucl. Sci. Technol. 40 (2003) 895.
[11] M. Futakawa, T. Wakui, H. Kogawa, Y. Ikeda, Nucl. Instrum. and Meth. A 562 (2006) 676.
[12] P. Bourdon, R. Simoneau, J.M. Dorey, in: Proceedings of the 17th IAHR Symposium, 1994, pp. 599–615.
[13] H. Soyama, R. Oba, K. Uranishi, H. Kato, in: Proceedings of International Symposium on Cavitation, 2005, p. 225.
[14] H. Soyama, M. Futakawa, Tribol. Lett. 23 (1) (2006) 23.
[15] M. Futakawa, T. Naoe, H. Kogawa, Y. Ikeda, J. Nucl. Sci. Technol. 41 (2004) 1059.
[16] B. Riemer et al., WS on the Pressure Wave Mitigation Technology, JAEA, Tokai, Japan, March, 2006.
[17] K. Okita, Y. Matsumoto, S. Takagi, in: Proceeding of FEDSM2005, 2005.
[18] H. Kogawa, S. Ishikura, H. Sato, M. Harada, S. Takatama, M. Futakawa, K. Haga, R. Hino, S. Meigo, F. Maekawa, Y. Ikeda, J. Nucl. Mater. 343 (2005) 81.
[19] N. Tanaka, K. Akutsu, M. Futakawa, Nucl. Instrum. and Meth. A 562 (2006) 680.
[20] M. Futakawa, T. Naoe, N. Tanaka, in: Proceedings of the 13th ICEM, 2007, p. 301.